Carbohydrate Polymer Technologies and Applications 9 (2025) 100689

Contents lists available at ScienceDirect

Carbohydrate Polymer Technologies and Applications

journal homepage: www.sciencedirect.com/journal/carbohydrate-polymer-technologies-and-applications

In situ delivery of synthetic preimplantation factor using aldehyde-modified hyaluronic acid hydrogel with immobilized complexes of chondroitin sulfate derivatives

Tutut Habibah [a,b,*], Andrea Exnerová [a], Kristina Nešporová [a], Una FitzGerald [c], Abhay Pandit [c], Marek Ingr [b], Martin Pravda [a], Vladimír Velebný [a]

[a] Contipro a.s. Dolní Dobrouč 401, Dolní Dobrouč, 56102, Czech Republic
[b] Faculty of Technology, Tomas Bata University in Zlín, Vavrečkova 5669, Czech Republic
[c] CURAM, Research Ireland Center for Medical Devices, University of Galway, Upper Newcastle, H91 W2TY, Ireland

ARTICLE INFO

Keywords:
Hydrogel
Synthetic preimplantation factor
Hyaluronic acid, Chondroitin sulfate
Polyelectrolyte complexes

ABSTRACT

Synthetic preimplantation factor (SPIF) is a promising therapeutic agent for chronic inflammatory diseases like Multiple Sclerosis (MS), but frequent systemic dosing limits patient adherence and therapy efficacy. This study presents an injectable drug delivery system (DDS) using 2 % (w/v) aldehyde-modified hyaluronic acid (HAOX) and chondroitin sulfate (CSOX) to deliver 100 μg of Fluorescein isothiocyanate-modified SPIF (FITC-SPIF). The DDS utilizes electrostatic interactions between the negatively charged sulfate groups of CSOX and the positively charged amino acids of FITC-SPIF for effective entrapment. Key properties were analyzed, including moderate gelation time (193 s), swelling profile (18 %), injectability (27 G needle) and an established relevant release profile (20 μg/daily ± 3) via anomalous diffusion. Increasing CSOX concentration reduced initial burst release by 38 % (0.5 % CSOX) to 78 % (1 % CSOX), extending release time (T50 %) from 50 h (0.5 % CSOX) to 88 h (1 % CSOX). Additionally, the release of FITC-SPIF enhanced TGF-β secretion in THP-1 macrophages, indicating preserved biological activity. These findings highlight the tunable release and mechanical properties achieved by adjusting the HAOX:CSOX ratio, strategically aligning the DDS for targeted MS symptom management. This system potentially simplifies SPIF delivery and enhances therapeutic efficacy.

Introduction

MS is a long-term demyelinating disease of the central nervous system (CNS) marked by the abnormal translocation of inflammatory cells across the blood-brain barrier (BBB). This process is driven by cytokines such as TGF-β, TNF-α, and IFN-γ (Meyer-Arndt et al., 2023; Ma et al., 2023), which trigger immune responses that lead to macrophage polarization and the recruitment of B-cells and T-cells, significantly contributing to MS pathogenesis (Touil et al., 2023; Häusser-Kinzel & Weber, 2019). While several disease-modifying therapies (DMTs) have been approved, their effectiveness is often limited by inadequate BBB penetration (Wu et al., 2023; Correale et al., 2021), particularly in patients with rapid disease progression.

Recent studies highlight the potential of SPIF, a 15-amino acid peptide derived from pregnancy, in treating neuroinflammatory conditions such as MS (Weiss et al., 2012; Hayrabedyan et al., 2019; Barnea et al., 2012). SPIF can cross the BBB (Spinelli et al., 2020), mitigate neurodegeneration, and reduce inflammatory responses (Weiss et al., 2012; Hayrabedyan et al., 2019; Spinelli et al., 2020). However, current delivery strategy in clinical (O'Brien et al., 2018; Di Simone et al., 2017) and preclinical trials (Hayrabedyan et al., 2019; Spinelli et al., 2020; Di Simone et al., 2017) primarily rely on systemic administration, necessitating frequent dosing to maintain therapeutic levels. This approach can lead to systemic toxicity and poor patient adherence (Barone et al., 2016; Lin et al., 2023; Visser et al., 2021), as the burden of multiple daily doses increases the risk of missed doses and treatment failure (Visser et al., 2021). The fragility and short biological half-life of peptides like SPIF further complicate effective delivery (Cavaco et al., 2021; Wang et al., 2022). Therefore, effective strategies are necessary for optimizing CNS delivery and improving drug efficacy (Barone et al., 2016; Lin et al., 2023; Visser et al., 2021).

This study develops an injectable DDS featuring immobilized

* Corresponding author.
E-mail address: habibahtutut@gmail.com (T. Habibah).

https://doi.org/10.1016/j.carpta.2025.100689

Available online 28 January 2025

polyelectrolyte complexes (PEC) formed from FITC-SPIF and CSOX (Fig. 1a). The PEC simplifies drug entrapment via electrostatic interactions, eliminating FITC-SPIF conjugation that may compromise drug integrity or lead to the formation of prodrugs. The crosslinkable system of HAOX and CSOX by O,O'−1,3-propanediylbishydroxylamine (PDHA) has been confirmed as biocompatible in prior studies (Toropitsyn et al., 2023; Buffa et al., 2015; Habibah et al., 2024; Bobula et al., 2016; Šedová et al., 2022), ensures safety and limit potential side effects. This system is engineered to provide sustained release of FITC-SPIF while maintaining its bioactivity.

The primary objective of this study is to develop a controlled release platform for FITC-SPIF that adapts to the biological parameters associated with MS. Previous research has often focused on inflammatory modulation or neuroprotection without effectively integrating pharmacodynamic aspects. This study aims to overcome limitations related to drug stability and delivery challenges, thereby advancing treatment options for MS through a DDS that potentially addresses the shortcomings of earlier investigations.

Materials and method

Materials

The materials used in this study included HAOX (HAOX25, Mw 325 kDa, DS 7.1 %) from Contipro a.s. (Czechia), FITC-6-Aminohexanoic acid-SPIF (FITC-Ahx-MVRIKPGSANKPSDD, PEP0235) from Iris Biotech (Germany), and bovine CS (CS, 10–40 kDa, C4S/C6S ratio 4/6) from Bioiberica (Spain). Additional reagents included 4-Acetamido-2,2,6,6-tetramethyl-piperidine-1-oxyl (4-AcNH-TEMPO) and O,O′−1,3-propanediylbishydroxylamine (PDHA, 98 %) from Sigma-Aldrich (Czechia), ethanol and sodium bromide from Lach-ner (Czechia). THP-1 cells (TIB-202™, ATCC), RPMI medium, fetal bovine serum (FBS-12A), d-glucose, penicillin/streptomycin, sodium pyruvate, phorbol 12-myristate-13-acetate (PMA), TNF-alpha, RNeasy Mini Kit, High-Capacity cDNA Reverse Transcription Kit, and quantitative reverse transcription polymerase chain reaction (qPCR) probes (GAPDH, TGF-β1, IL-10, CXCL8, PTGS2, IL1b, TNF alpha) were sourced from various suppliers, including Biosera, Capricorn Scientific, Merck, Sigma-Aldrich, QIAGEN, and ThermoFisher. Normal saline (0.9 % w/v NaCl, prepared in-house using 9 g of non-iodized salt dissolved in 1 L of sterile deionized water).

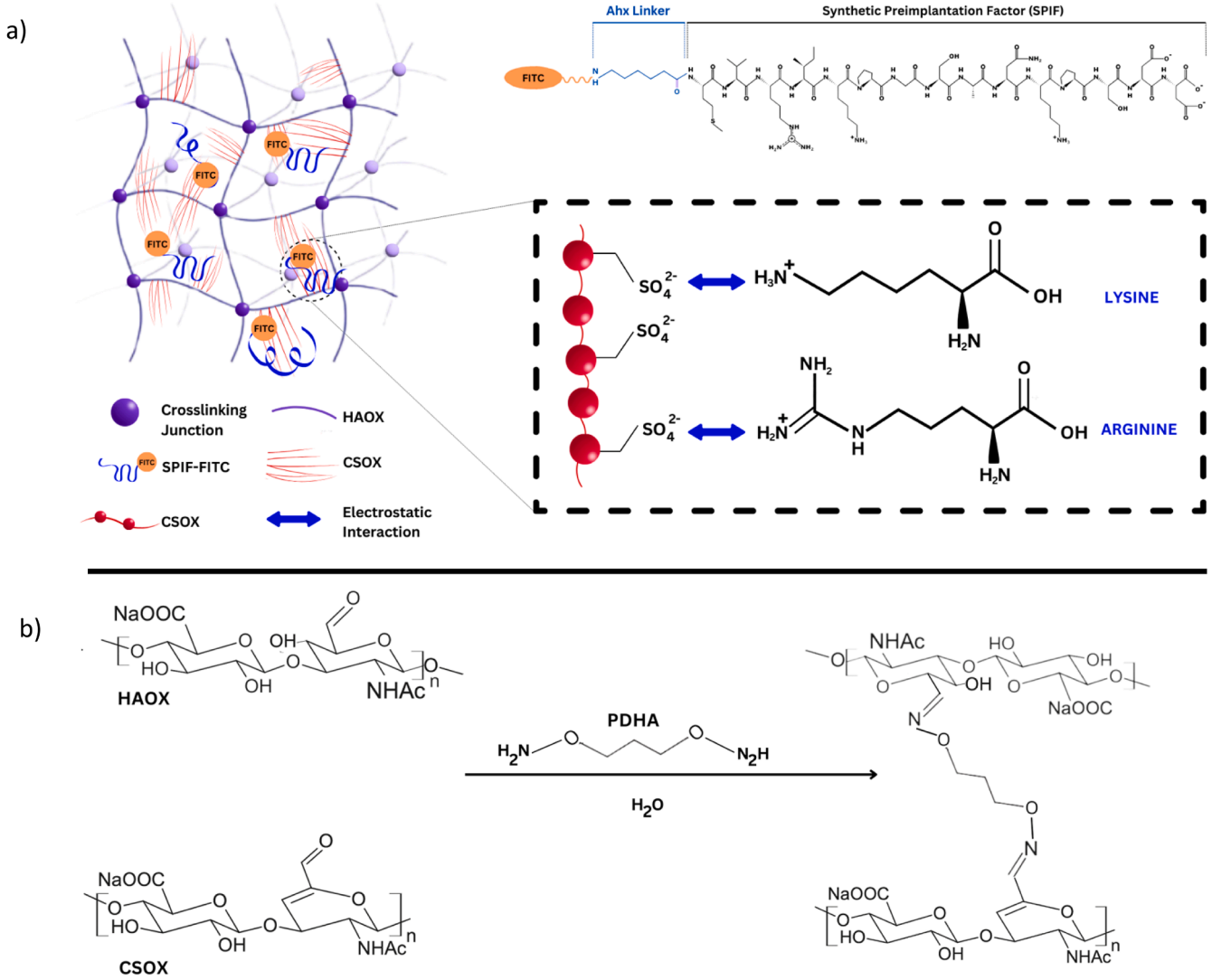

Fig. 1. a) DDS for SPIF based on HAOX:CSOX with the formation of the PEC is driven by the electrostatic attraction between the negatively charged sulfate groups of the CSOX and the positively charged amino and guanidino residues of FITC-SPIF, b) the crosslinking reaction of the modified disaccharidic units of CSOX and HAOX polymers with the PDHA.

Synthesis of aldehyde-modified chondroitin sulfate

CSOX was synthesized using a modified protocol (Habibah et al., 2024; Bobula et al., 2018). First, 1040 mg of CS (2 mmol, 1 equiv.) was dissolved in 52 mL of deionized water (2 % w/v) along with 400 mg of disodium phosphate (1 mmol) and 103 mg of NaBr (1 mmol, 0.5 equiv.). After adding 4 mg of 4-AcNH-TEMPO (0.02 mmol, 0.01 equiv.), the solution was cooled to 5 °C ± 1. Next, 560 μL of NaClO (11 % active chlorine, 1 mmol, 0.5 equiv.) was added, and the mixture was stirred for 30 mins at 5 °C ± 1. The reaction was quenched with 10 equivalents of ethanol and dialyzed using a 14 kDa MWCO cellulose membrane (D9527, Sigma Aldrich). The dialysis product (10 mL ± 2) was then frozen at −80 °C ± 1 for 24 h (TSX Universal Series ULT freezers, Thermo Scientific). Frozen samples were transferred to the drum manifold of a freeze-dryer (Labconco FreeZone 4.5 L Benchtop 710,402, 090, Thermo Scientific). Primary drying was conducted at an ambient temperature of 25 °C ± 1 for 48 h, with the condenser temperature set to −105 °C ± 3 and the pressure maintained at 10 μbar ± 0.5. After freeze-drying, 20 mg of the obtained fibers were dissolved in 20 mL of D2O for ^{1}H NMR analysis (Bruker Avance Neo 700 MHz). The degree of functionalization (DF) was determined using ^{1}H NMR spectroscopy, revealing a DF of approximately 20 %, with 80 % of the repeating units remaining sulfated to support PEC formation. Analysis by Size-Exclusion Chromatography coupled with Multi-Angle Laser Light Scattering (SEC-MALLS) confirmed the molecular mass of M_{CSOX} as 12 kDa, indicating successful synthesis.

Formulation of hydrogel

The hydrogel-based DDS were prepared through covalent crosslinking of aldehyde groups from HAOX or CSOX with hydroxylamine from PDHA. The polymers were dissolved in normal saline with FITC-SPIF, and the pH was maintained at 5.0 ± 0.2 or 6.8 ± 0.2 using HCl. The PDHA solution was then adjusted to pH 7.0 ± 0.2 with NaOH. Crosslinking was performed using a two-component syringe system (Fig. S1a), with detailed formulations provided in Table 1. Two preparation methods with varying pH levels and HAOX-to-CSOX ratios (totaling 2 % polymer by weight) were employed: one involving only HAOX and PDHA as a control (HAOX-based hydrogel), and another incorporating HAOX and CSOX crosslinked by PDHA to facilitate immobilized PEC formation. Adjusting the preparation pH aimed to increase the charge density of FITC-SPIF's amine residues, promoting stronger interactions with CSOX sulfate groups to enhance drug entrapment and enable a controlled release mechanism.

Preparation of HAOX-based hydrogel (HAOX_15 and HAOX_17)

HAOX was dissolved in normal saline at 60 °C ± 1 for 3 h and stirred overnight at 25 °C ± 1. Simultaneously, 150 mg of PDHA was dissolved in 10 mL of normal saline at 25 °C ± 1, with the pH adjusted to 7.0 ± 0.2 using NaOH. A two-component syringe system was utilized for crosslinking, with one syringe containing the HAOX solution and the other containing PDHA. The solutions were mixed in equal volumes to achieve a total polymer concentration of 20 mg mL^{-1} in the crosslinked hydrogel for each formulation. The mixture was then transferred to a Teflon mold. The required amount of PDHA (C_{PDHA}) for crosslinking was calculated based on a 1:1 ratio of aldehyde to hydroxylamine groups, as described in Eq. (1). In this equation, C_{HAOX} represents the polymer concentration (w/v) of HAOX, DS_{HAOX} denotes the substitution degree of HAOX, P is set to 1 (indicating the ratio of aldehyde to hydroxylamine groups), P_p indicates the number of hydroxylamine groups in PDHA (2), V_{HAOX} is the volume of HAOX solution in the first syringe, V_{PDHA} is the total volume of the PDHA solution in the second syringe, M_{PDHA} is the molecular weight of PDHA (179 g mol^{-1}), and M_{HAOX} is the molecular weight of the HA disaccharide unit (400 g mol^{-1}).

$$C_{PDHA} = \frac{C_{HAOX} \cdot V_{HAOX} \cdot M_{PDHA} \cdot DS_{HAOX}}{V_{PDHA} \cdot P \cdot P_p \cdot M_{HAOX}} \quad (1)$$

Preparation of HAOX containing immobilized CSOX (HAOX_25, HAOX_35, HAOX_27, and HAOX_37)

HAOX and CSOX were simultaneously dissolved in the same vessel of normal saline containing FITC-SPIF. The pH was adjusted to 5.0 ± 0.2 or 6.8 ± 0.2, and the solution was heated to 60 °C ± 1 for 3 h, followed by overnight stirring at 25 °C ± 1. The crosslinking process adhered to standard procedures, with the required amount of PDHA calculated using Eq. (2) to maintain a 1:1 ratio of crosslinkable aldehyde and hydroxylamine groups from HAOX and CSOX (Fig. 1b), considering their respective molecular weights. The quantities in the second set of parentheses correspond to the CSOX equivalents, where M_{CSOX} denotes the molecular weight of the CS disaccharide unit (600 g mol^{-1}).

$$C_{PDHA} = \left(\frac{C_{HAOX} \cdot V_{HAOX} \cdot M_{PDHA} \cdot DS_{HAOX}}{V_{PDHA} \cdot P \cdot P_p \cdot M_{HAOX}}\right) + \left(\frac{C_{CSOX} \cdot V_{CSOX} \cdot M_{PDHA} \cdot DS_{CSOX}}{V_{PDHA} \cdot P \cdot P_p \cdot M_{CSOX}}\right) \quad (2)$$

Gelation time

The gelation time of the HAOX gel was studied using a Discovery Hybrid Rheometer–3 (TA Instruments) with a plate-plate setup (40 mm diameter plate, 400 μm gap). After the addition of the cross-linking agent, the real-time elastic (G′) and viscous (G″) moduli were measured. Viscoelastic properties were assessed through a 180 s oscillatory time sweep at 25 °C, using a 5 % constant strain and an angular frequency of 6.283 rad s^{-1} (1.0 Hz), with a 6 s sampling interval. Next, the gel-forming solution (0.5 mL) was applied to the Peltier plate, followed by the addition of a 0.5 mL PDHA solution. A 2000 s^{-1} pre-shear for 3 s homogenized the solutions and initiated gelation. The gelation time, which marks the crossover points of the G′ and G″ curves from viscous to elastic behavior, was determined. Measurements were conducted in triplicate and averages with standard deviations were calculated.

Swelling ratio

The swelling ratio (Q) of the drug delivery system (DDS) was calculated using Eq. (3):

$$Q = \frac{(m_t - m_r)}{m_r} \times 100\% \quad (3)$$

In this study, m_t represents the mass of the hydrogel after swelling, while m_r denotes the mass of the hydrogel in its initial relaxed state. A volume of 1 mL from each crosslinked DDS was transferred to the insert (25 mm diameter; 3 μm pore size) of a 12-well Transwell® system (Corning, Inc., Acton, MA), which contained 2 mL of PBS 7.4 as the swelling medium in the apical compartment. The entire system was incubated in a Witeg Wisd Incubator (WITEG Labortechnik, Germany) at

Table 1
Formulations for FITC-SPIF DDS, including HAOX-based DDS and HACOX (HAOX and CSOX-based DDS) at two different preparation pH levels.

Formulations	HAOX (mg mL^{-1})	CSOX (mg mL^{-1})	FITC-SPIF (μg mL^{-1})	PDHA (mg mL^{-1})	Preparation pH
HAOX_15	20	0	100	0.32	5.0
HACOX_25	15	5	100	0.39	5.0
HACOX_35	10	10	100	0.465	5.0
HAOX_17	20	0	100	0.32	6.8
HACOX_27	15	5	100	0.39	6.8
HACOX_37	10	10	100	0.465	6.8

37 °C ± 1 and 96 % ± 0.5 relative humidity. At predetermined intervals (1, 3, 7, and 14 days), the hydrogel was weighed at 25 °C ± 1 (ME103, Mettler Toledo, Switzerland). After weighing, the medium was aspirated from the apical compartment and replenished with 2 mL of fresh PBS 7.4 solution before returning the hydrogel to the Transwell® system.

FITC-SPIF release experiment and release fitting model

To investigate the in vitro release of FITC-SPIF from the DDS, the Transwell® drug release method was utilized. A 1 mL sample of cross-linked hydrogel was placed onto a semi-permeable polyester membrane (25 mm diameter; 3 μm pore size) in the donor compartment of a 12-well Transwell® system (Corning, Inc., Acton, MA). The apical compartment contained 2 mL of PBS at pH 7.4 as the release medium. The system was incubated in a Witeg Wisd Incubator (WITEG Labortechnik, Germany) at 37 °C ± 1 and 96 % ± 0.5 relative humidity. The release medium was refreshed every 24 h, and the concentration of FITC-SPIF was quantified using UV–Vis spectroscopy. Cumulative drug release (CDR) was calculated using Eq. (4). Detailed procedures for limits of detection and quantification are provided in the Supplementary Information.

$$\mathrm{CDR} = \frac{m_t}{m_\infty} \text{ x } 100\% \tag{4}$$

m_t is the amount of drug released at a given time, and m_∞ is the total mass of the drug loaded. The release mechanism of FITC-SPIF was analyzed using the Korsmeyer–Peppas (Korsmeyer et al., 1983) model, as described in Eq. (5).

$$\mathrm{k}t^n = \frac{m_t}{m_\infty} \tag{5}$$

Using the model, we determined the release exponent (n) and kinetics constant (k), reflecting the system's structural and geometric characteristics. The parameters (m_t) and (m_∞) were used as described in Eq. (4).

Injectability

To evaluate the ease of injection (Alonso et al., 2021), 27 G needles and a two-syringe system with a luer-lock adapter were used following established protocol with modifications (Toropitsyn et al., 2023; Habibah et al., 2024). The first syringe contained a polymer solution with FITC-SPIF, and the second contained PDHA. After mixing in a 50:50 ratio for 10 s, the mixture was tested with an Instron 3342 single-column materials testing system. The injection force was measured using a 100 N compression plate at 50 mm/min. Bluehill software recorded data on injection force, plunger displacement, dynamic glide force (*DGF*), and (F_{max}), with measurements repeated thrice and results presented as averages with standard deviations for the values obtained at 60 s and 180 s to show the injectability profile across a range of time points.

Elastic limit and strain limit

The viscoelastic properties of the hydrogels were evaluated to determine their suitability for drug delivery applications, focusing on factors such as mechanical stability (Stojkov et al., 2021). Measurements were performed using a Discovery Hybrid Rheometer-3 at 25 °C with a 20 mm stainless-steel plate, following a modified protocol from Toropitsyn et al. (2023). Oscillatory strain sweep tests determined the limit (γL) of the linear viscoelastic region (LVE) and measured the storage moduli (G′) and the loss moduli (G″). The samples were subjected to sinusoidal oscillatory strain at 1 Hz (6.28 rad s^{-1}) with amplitudes ranging from 0.001 to 2.0 rad. γL was identified as the strain at which G′ becomes stress-dependent. G′ values were maintained within ± 5 % of the plateau value, and mean G′ and G″ values were computed from the LVE region.

Mesh size, $\mathbf{M_c}$, and cross-linking density

The influence of HAOX:CSOX concentration on hydrogel structure was analyzed by determining M_c through Peppas' theory (Peppas et al., 2000) and calculating mesh size (ξ) using rubber elasticity theory as formulated by Flory (Flory, 1953). This theory elucidates the relationship between swelling and structure, where M_c correlates with ξ, defining the average distance between adjacent cross-links in a swollen hydrogel. ξ was calculated using the Eq. (6):

$$\xi = \mathrm{l}v_{2,s}{}^{-\frac{1}{3}}\left(\frac{2C_nM_c}{M_r}\right)^{\frac{1}{2}} \tag{6}$$

The virtual bond length l, defined as the distance between glycosidic oxygens within a monosaccharide, spans 0.52 nm for HAOX (Martini et al., 2016) and 0.48 nm for CSOX (Tanaka, 1978). The Flory characteristic ratio C_n is 27 for HAOX (Martini et al., 2016) and 15.705 for CSOX (Tanaka, 1978), while M_r represents the molecular weight of the repeat disaccharide unit, which is 400 g mol^{-1} for HA and 600 g mol^{-1} for CSOX. M_c and ξ values incorporate the structural contribution of CSOX based on the volume fraction of the monomer present in the formulation. Detailed ξ calculation and $v_{2,s}$, are in the Supplementary Information section (c).

FITC-SPIF effect on cytokines expression

The bioactivity of FITC-SPIF in DDS was assessed using an inflammation model with THP-1 macrophages, with the following modifications (Chen et al., 2016). THP-1 cells were cultured in RPMI medium with 10 % FBS, d-Glucose (4.5 g/L), l-Glutamine (2 mM), Penicillin/streptomycin (100 U/mL), and Sodium Pyruvate (1 mM) under 37 °C ± 0.5 and 5 % ± 0.3 CO_2 (Heracell™ VIOS 160i CO_2 Incubator, 165 L). The cells were differentiated into macrophage-like cells following exposure to 100 nM PMA for 72 h then rested for 24 h in complete media without PMA. Post-differentiation, cells were pre-treated with FITC-SPIF alone or FITC-SPIF released from the DDS for 48 h. Activated macrophages were stimulated with tumor necrosis factor alpha (TNF-α) (100 ng ml^{-1}). Samples for qRT-PCR analysis were obtained in triplicate at specified intervals: 0 h (following 48 h incubation with FITC-SPIF, pre- TNF-α application), and 6 h (48 h incubation with FITC-SPIF samples followed by 6 h with TNF-α). qRT-PCR analysis was conducted on each cDNA sample for the assessment of gene expression, focusing on the activation of IFN-γ (Chen et al., 2016), and other proinflammatory genes (CXCL8, PTGS2, TNF, IL-6, IL-1b), as well as anti-inflammatory genes (IL-10, TGF-β). Threshold cycle (CT) values were computed relative to the housekeeping gene GADPH.

Data and statistics analysis

All experiments were conducted in triplicates to ensure reliability. Statistical analyses were performed using one-way analysis of variance (ANOVA), with a significance threshold set at $p < 0.05$. To examine the linear relationship between continuous variables, Pearson correlation and linear regression analyses were employed. These tests assessed the presence and strength of statistically significant correlations between the variables.

Results and discussion

Gelation time, injectability, and viscoelasticity of the delivery system

The performance of injectable DDS is critically influenced by interrelated properties such as gelation time, injectability, and mechanical strength (Salehi et al., 2023; Bernhard & Tibbitt, 2021; Kesharwani et al., 2021; Lei et al., 2022). These characteristics are critical for effective administration and the integrity of hydrogels post-injection.

Current study evaluated the gelation time of DDS using rheological measurements (Fig. 2a), revealing a transition from liquid to solid state upon mixing with the crosslinking agent PDHA. The gelation times varied significantly with pH; formulations at pH 5 exhibited consistent gelation times averaging 74 s, while those at pH 6.8 showed slower kinetics, ranging from 70 s to 193 s ($p < 0.01$). This variability underscores the importance of pH in influencing gelation rates, which are crucial for preventing leakage during injection and ensuring localized system (Toropitsyn et al., 2023; Grover et al., 2012).

Faster gelation, particularly under acidic conditions, accelerates oxime linkage formation by forming a more uniform distribution of crosslinked sites within the hydrogel matrix (Grover et al., 2012; Collins et al., 2016), thereby preventing premature drug release and polymer leaching. However, it may also lead to needle clogging during injection. HAOX-based DDS systems typically demonstrate gelation times around one minute, aligning with previous studies (Toropitsyn et al., 2023; Habibah et al., 2024). While acid-catalyzed oxime formation can expedite gelation, physiological conditions often necessitate crosslinking at neutral pH (Zhang et al., 2018), as evidenced by our findings of a 193-second gelation time at pH 6.8. Notably, a gelation period of 3–5 mins is considered optimal for injectable hydrogels to conform to tissue cavities and ensure an effective interface (Tseng et al., 2015; Zhuo et al., 2017; Niemczyk et al., 2018).

The injectability of HACOX_37 was evaluated using a two-syringe system, which demonstrated that a gelation time of 3–5 mins facilitated smooth injection through a 27 G needle (Table 2). The small needle size is advantageous, as it ensures minimal perforations in the implanted device, thereby enhancing patient comfort. HACOX_37 was specifically chosen for its favorable gelation time, which allowed it to maintain sufficient fluidity during administration while achieving adequate viscosity after injection. The formulation exhibited a maximum force (Fmax) of 172 KPa at 60 s post-crosslinking, which increased to 185 KPa at 180 s, indicating a moderate rise in viscosity. Importantly, The Dynamic Glide Force (DGF) required to move the pre-mixed hydrogel through the syringe was consistently below 40 N, within acceptable limits (Alonso et al., 2021).

Mechanical testing revealed that the viscoelastic properties of the hydrogels could be optimized by adjusting CSOX concentration and crosslinking density (Fig. 2b). The rheological analysis indicated that the G′ within the LVE region reflects the strength of the DDS, with higher values suggesting greater durability. For instance, HAOX_17 exhibited a strength of approximately 1083.7 Pa, while increasing CSOX concentration significantly reduced this strength due to ineffective crosslinking within the DDS. This reduction in strength correlates with increased swelling capacity, highlighting the delicate balance between crosslinking density and hydrogel performance. Overall, our findings emphasize the critical interplay between gelation time, injectability, and mechanical properties in the design of effective injectable DDS.

Table 2
Injectability of HACOX_37 ($n = 3$).

Formulation	needle size (G)	Duration from crosslinking process (s)	DGF (N)	Fmax (Kpa)
HACOX_37	27	60 180	2.8 2.89	172 185

Swelling ratio

The swelling behavior of hydrogels in water or physiological fluids is largely determined by osmotic pressure, which arises from the hydrophilicity of the polymers, static charges, and counter ions (Berradi et al., 2023; Feng & Wang, 2023). Swelling triggers volume phase transitions that influence drug release profiles, and this can be tailored by modifying the hydrogel's size, shape, and cross-linking density (Buenger et al., 2012). Evaluating the swelling ratio in cross-linked hydrogels is crucial for assessing cross-linking efficiency and the ability to control drug release kinetics. Low swelling capacity is particularly desirable for drug delivery applications (Xue et al., 2020).

The dynamic swelling profile of HAOX_17, HACOX_27, and HACOX_37 was measured by immersing samples in PBS and recording weight changes. Both dynamic and equilibrium swelling ratios were assessed using a constant polymer concentration of 2 %. Fig. 3 illustrates the effect of CSOX concentration on hydrogel swelling. Initially, HAOX_17 exhibited a reduction in weight during the first 24 h likely due to higher HAOX concentration which supports effective crosslinking formation and thus increases crosslink density and reduces network expansion. Conversely, higher CSOX concentrations in HACOX_27 and HACOX_37 resulted in increased swelling, attributed to the hydrophilic hydroxyl (–OH) and sulfate ($–SO_3$) groups in CSOX, which enhance polymer hydration (Samantray et al., 2021; Tao et al., 2012). Increased water uptake can delay drug release by retaining water within the hydrogel structure, rather than promoting drug diffusion (Novoskol'tseva et al., 2009).

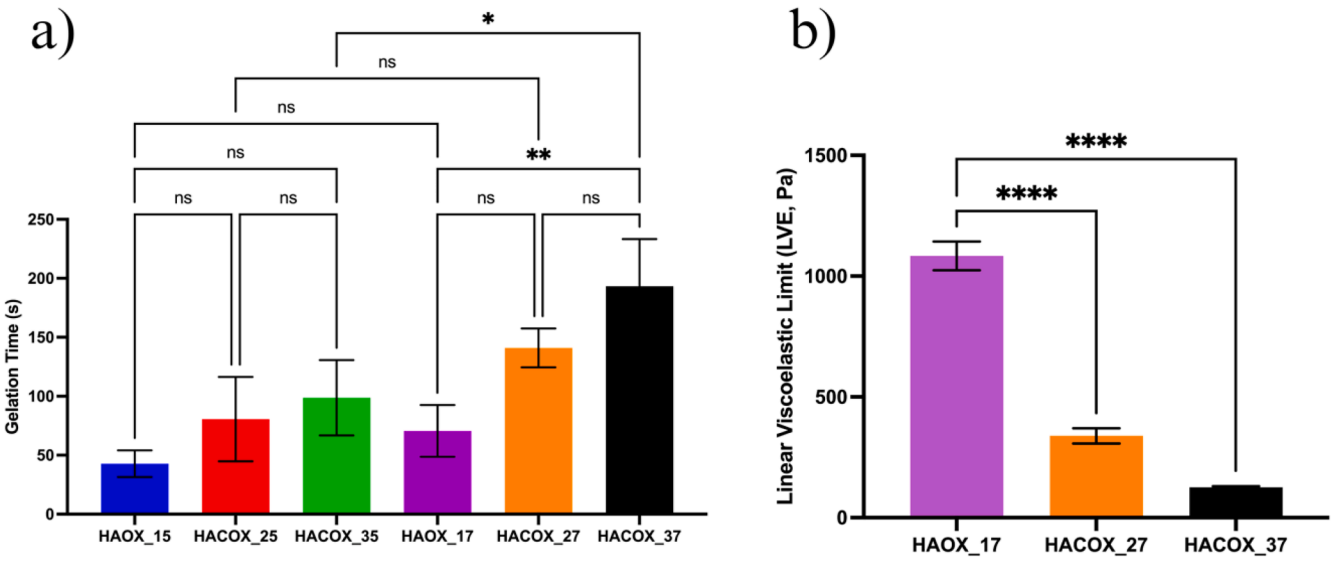

Fig. 2. a) Gelation duration of formulation prepared at pH 5 (HAOX_15, HACOX_25, and HACOX_35, $n = 3$), and pH 6.8 (HAOX_17, HACOX_27, and HACOX_37), b) Strength of DDS depicted as the limit of G' in LVE. ($n = 3$), * $p < 0.05$, ** $p < 0.01$, ***$p < 0.001$, ****$p < 0.0001$, ns = non-significant.

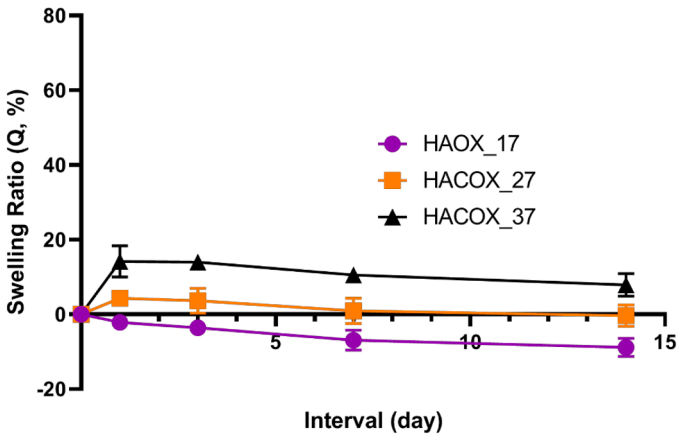

Fig. 3. Swelling profile of delivery system prepared at pH 6.8 ($n = 3$).

Studies consistently report low swelling ratios for HAOX_17, HACOX_27, and HACOX_37, ranging from 1 % to 20 %, indicating minimal structural expansion and supporting sustained, controlled drug delivery (Toropitsyn et al., 2023; Buffa et al., 2015). Our experiments employed Transwell® inserts to simulate an implanted reservoir, restricting hydrogel exposure to surrounding fluids and causing uneven swelling and deswelling kinetics (Lin et al., 2009; Mihajlovic et al., 2022). Additionally, crosslinking junctions within the hydrogel, coupled with confinement, act as retractive forces, limiting structural expansion (Dulong et al., 2004; Shimojo et al., 2015). The equilibrium swelling ratio was determined when the hydrogel achieved constant weight, typically commenced after 7 days.

FITC-SPIF release

UV–Vis analysis demonstrated consistent release kinetics across pH conditions, with higher CSOX concentrations decreasing the initial burst release and promoting a slower, sustained release (Fig. 4a). In the first 24 h, the control DDS with only HAOX at pH 5 released approximately 43 μg of FITC-SPIF (HAOX_15), followed by an average release of 20 μg. The same system at pH 6.8 (HAOX_17) similarly showed an initial release of 44 μg, followed by approximately 18 μg.

Incorporating 0.5 % CSOX into the HAOX matrix (HACOX_25 and HACOX_27) significantly reduced burst release by 40 % for HACOX_25, with a subsequent release of 18 μg, and by 38 % for HACOX_27, yielding 15 μg ($p < 0.05$). Increasing CSOX concentration to 1 % further decreased burst release by 58 % for HACOX_35 ($p < 0.01$), with an average subsequent release of 14 μg, and by 78 % for HACOX_37 ($p < 0.001$), with a release of 13 μg. The time to achieve 50 % release of FITC-SPIF (T50 %) indicated release retardation (Fig. 4b), with T50 % values of approximately 28.5 h ± 2.1 for HAOX-based DDS, 52.5 h ± 3.1 for HACOX_25 and HACOX_27, 70.4 h ± 6.2 for HACOX_35, and 88.0 h ± 5.4 for HACOX_37. The significant reduction in burst release and extended T50 in HACOX_37 establishes a benchmark for further optimization. Furthermore, the formulations effectively released FITC-SPIF at rates between 1 and 20 μg daily, consistent with the lower dosing ranges observed in preclinical and clinical studies. In a murine model (Di Simone et al., 2017), SPIF was administered at 1 μg g^{-1} mouse per day, totaling 20 μg for a 20 g mouse. Similarly, a Phase I clinical trial indicated doses for an average adult weighing 70 kg ranged from approximately 7 μg kg^{-1} to 70 μg per dose (O'Brien et al., 2018). This suggests that the formulation operates at clinically relevant doses while offering a more controlled and sustained release compared to traditional single dosing regimens.

The primary mechanism for sustained FITC-SPIF release involves interactions between the strong anionic sulfate groups in CSOX and the weak cationic groups in FITC-SPIF amino acid residues. Variations in burst release may be attributed to the nature of PEC reactions, comprising ion pairs and undissociated components (Mikulík et al., 1993; Gummel et al., 2007; Shah & Leon, 2021). Ion pairs form a complex that functions as a reservoir, delaying FITC-SPIF release through binding to sulfate groups, while unbound FITC-SPIF is rapidly released, contributing to higher burst release levels (Mikulík et al., 1993). Burst release is often detrimental in extended DDS applications due to potential local toxicity, increased dosing frequency, and economic waste (Huang & Brazel, 2001). Studies indicate that PECs can form in less than 5 milliseconds under specific mixing conditions (Schatz et al., 2004), and longer gelation times in DDS formulations allow sufficient time for PECs to achieve structural stability.

The crosslinking of PECs within the HAOX network and the presence of adequate functional groups contribute to a stable environment for loaded FITC-SPIF, thereby regulating its immediate release. Controlled release is critical for minimizing burst effects and ensuring prolonged therapeutic effectiveness. For HAOX_15 and HAOX_17, the observed

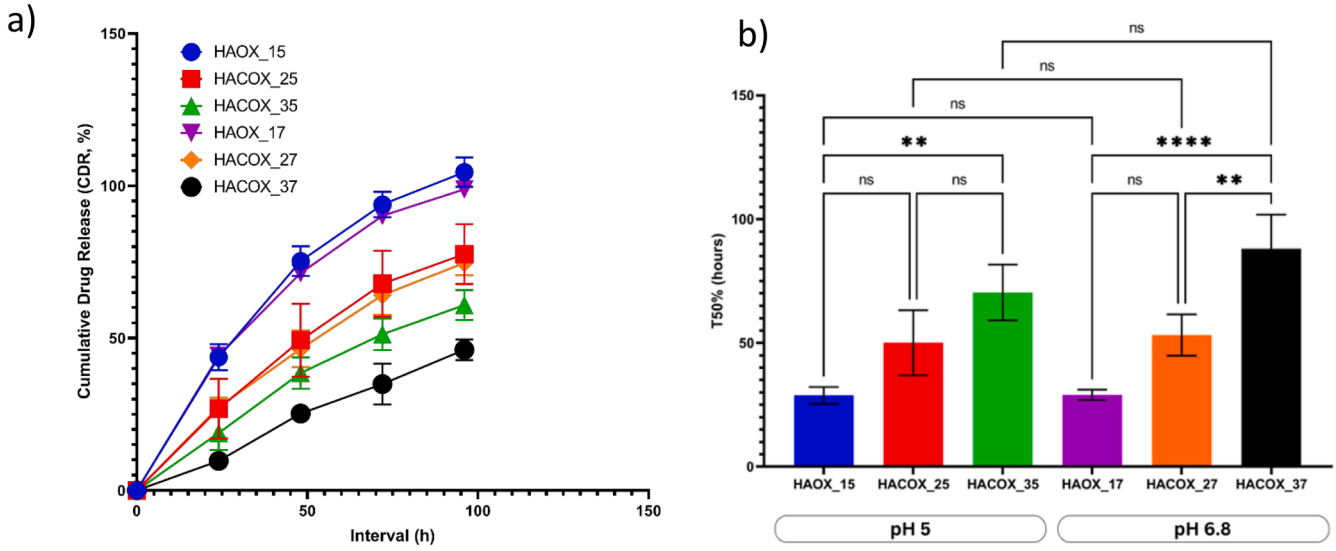

Fig. 4. Release profile of FITC-SPIF across formulations, a) Cumulative Drug Release (CDR) and b) T50 % of formulation prepared at pH 5 (HAOX_15, HACOX_25, and HACOX_35), and pH 6.8 (HAOX_17, HACOX_27, and HACOX_35), and pH 6.8 (HAOX_17, HACOX_27, and HACOX_37) with $n = 3$, $^{*}p < 0.05$, $^{**}p < 0.01$, $^{***}p < 0.001$, $^{****}p < 0.0001$.

release profile suggests that FITC-SPIF molecules are smaller than the hydrogel mesh size, resulting in nearly 100 % drug release and the highest burst release among all formulations. In contrast, higher concentrations of CSOX in the formulation increase interaction sites for FITC-SPIF, facilitating more efficient entrapment and advantageous for stable, prolonged drug release.

The influence of varying pH levels on complex formation considers the presence of H^+ions, which are abundant in lower pH environments and affect the degree of neutralization of polyelectrolytes, influencing the degree of dissociation, and effective charge densities (Knoerdel et al., 2021; Qu et al., 2022). Fig. 4b shows that varying pH levels does not significantly impact burst release within the same formulations. The pH of all preparations remained below the pKa of the amine residue (approximately 10.8) (Marciel et al., 2017), and the guanidino group (approximately 13.8) (Fitch et al., 2015). Consequently, there was no significant difference in charge densities between the formulations, leading to comparable burst release outcomes.

The drug release behavior of hydrogels is influenced by various factors, including release capacity, time, rate, and diffusion mechanism (Ilgin et al., 2019; Modrzejewska et al., 2010). The Korsmeyer-Peppas kinetic model is commonly used to describe drug transport from polymeric matrices, particularly when multiple release mechanisms are involved or the mechanism is not fully understood (Korsmeyer et al., 1983; Modrzejewska et al., 2010).

The high coefficients of determination (R^2) ranging from 0.97 to 1.00 (Table 3) indicate a robust correlation within the experimental dataset. Increasing CSOX concentration in the DDS formulation significantly reduces transport constants (k), with HACOX_37 exhibiting the lowest value. The parameter k reflects constant drug transport, directly impacting release kinetics, where higher values denote faster release and lower values indicate slower kinetics.

Regardless of the preparation pH, the diffusional exponent values (n) in the range of $0.45 < n < 1$ suggest anomalous (non-Fickian) transport, indicating that FITC-SPIF release is governed not only by diffusion (Rungrod et al., 2022; Agarwal et al., 2021) but also by other factors such as solubility, crosslinking density, material composition, and interactions between FITC-SPIF and the components of the polymeric DDS (García-Couce et al., 2021). The Pearson correlation between swelling profile and T50 % suggests a negative relationship between released FITC-SPIF and water uptake (Fig. S3 in supplementary information). However, since the formulations exhibit low to no swelling (Xue et al., 2020), this effect is considered non-fundamental.

Additionally, the solubility of FITC-SPIF in saline and PBS can be ruled out as a determinant of release behavior. Analyzing material composition (Table 1), increased CSOX concentration in the matrix results in decreased FITC-SPIF release, while formulations with only HAOX (HAOX_15 and HAOX_17) show increased drug release. This aligns with previous observations where interactions between FITC-SPIF and sulfate groups delay drug release from matrices with higher COSX content. Mathematical modeling of drug release simplifies the complex process by focusing on dominant forces, though discrepancies between theory and experimental data are expected due to multiple contributing factors (Fu & Kao, 2010).

Variations in release profiles allow tailored treatment options based on therapeutic goals. For chronic MS management, sustained and controlled drug release maintains consistent levels, provides ongoing symptom relief, and may enhance patient compliance by reducing dosing frequency. Conversely, during acute exacerbations, immediate symptom relief and rapid inflammation control are vital, making a DDS enabling faster release to achieve higher initial concentrations preferable.

Table 3
Korsmeyer-Peppa data fitting of FITC-SPIF DDS across different preparation pH.

Formulations	k	n	R^2
HAOX_15	0.037	0.771	0.999
HACOX_25	0.020	0.819	0.999
HACOX_35	0.018	0.775	0.997
HAOX_17	0.049	0.690	1
HACOX_27	0.023	0.769	0.999
HACOX_37	0.008	0.900	0.997

Crosslinking density, molecular weight between crosslinks (M_c), and mesh size (ξ)

The mechanical and swelling properties of hydrogels, including drug diffusivity, are governed by structural characteristics such as crosslinking density, represented by the number of covalent bonds per unit volume (Lin et al., 2022; Lavrentev et al., 2023; Ho et al., 2022). Mesh size (ξ), the distance between cross-links, determines drug retention and release, influenced by polymer and crosslinker concentrations (Ho et al., 2022; Li & Mooney, 2016). Additionally, the average molecular weight between cross-links ($\mathbf{M_c}$) affects hydrogel flexibility and extensibility, increasing with the swelling ratio (Hoti et al., 2021).

Table 4 shows significant differences in crosslinking density among formulations, with HAOX_17 exhibiting the highest density at 8.656 mol mL^{-1}, likely due to efficient crosslinking, which reduces network expansion ($p < 0.0001$). Adding 0.5 % and 1 % CSOX (HACOX_27 and HACOX_37) lowers crosslinking density by 19 % and 38 %, respectively. This increase in CSOX concentration also reduces $\mathbf{M_c}$, from 141,970 g mol^{-1} in HAOX_17 to 135,903 g mol^{-1} in HACOX_27 and 126,350 g mol^{-1} in HACOX_37 ($p < 0.0001$). Similarly, ξ decreases as CSOX concentration increases ($p < 0.05$ for HAOX_17 vs HACOX_27; $p < 0.0001$ for HAOX_17 vs HACOX_37; $p < 0.05$ for HACOX_27 vs HACOX_37). Pearson correlation analysis found a significant negative relationship between the FITC-SPIF release profile and mesh sizes, which likely due to the significant differences in CSOX concentration which also contribute to ξ values, but not effective crosslinking formation ($p < 0.05$) (see supplementary information Fig. S5 section (d)).

The results show a negative correlation between CSOX concentration and $\mathbf{M_c}$, as well as crosslinking density. Similarly, DDS also exhibits the same correlation while displaying ξ values when compared to HAOX_17, which served as the control. Previous studies, where the comprehensive calculation, have shown that this reduced $\mathbf{M_c}$ is due to CSOX's lower $\mathbf{M_n}$ and density (Habibah et al., 2024). Additionally, CSOX tends to form branching structures rather than contributing significantly to crosslinking with HAOX, which enhances the hydrogel's water affinity by increasing the free volume (Tao et al., 2012; Takeno & Sato, 2016). Despite these structural differences, HAOX remains the primary factor influencing hydrogel mesh size, with shorter chain of CSOX showing limited contribution to network formation in the DDS.

In vitro FITC-SPIF bioactivity assay

Aberrant immune responses are central to MS pathogenesis, with Vascular Cell Adhesion Molecule-1 (VCAM-1) promoting leukocyte migration across the blood-brain barrier (BBB) (Yang et al., 2019; Takeshita & Ransohoff, 2012). Targeting VCAM-1 with FITC-SPIF is, therefore, a promising therapeutic approach. Preliminary experiments were conducted to assess the sustained activity of released FITC-SPIF by

Table 4
Crosslinking density, $\mathbf{M_c}$, and ξ of FITC-SPIF DDS prepared a pH 6.8 ($n = 3$).

Formulations	Crosslinking Density (mol mL^{-1})	$\mathbf{M_c}$ (g mol^{-1})	ξ (nm)
HAOX_17 (PURE HAOX)	8.656 ± 0.010	141,970 ± 254	299 ± 11
HACOX_27	7.003 ± 0.008	135,903 ± 162	247 ± 4
HACOX_37	5.338 ± 0.001	126,350 ± 29	201 ± 10

measuring its impact on VCAM-1 expression levels (Chen et al., 2016).

Non-activated THP-1 macrophages were pre-treated with 12.5 μg mL^{-1} of FITC-SPIF, either FITC-SPIF alone, or released from the DDS, for 48 h. Following this, macrophages were activated with TNF-α (100 ng mL^{-1}). Samples for qPCR analysis were collected at 0- and 6-h post-treatment to assess GAPDH and VCAM-1 gene expression. No inhibitory effect of released FITC-SPIF on VCAM-1 expression was observed compared to the control likely due to the cell line used (THP-1 versus RAW264.7). Results are detailed in the Figs. S6–S8 Supplementary Information section (e).

The impact of FITC-SPIF on proinflammatory (CXCL8, PTGS2, TNF, IL-6, IL-1β) and anti-inflammatory (IL-10, TGF-β) cytokine expression was also assessed. While proinflammatory gene expression remained unaffected, there was a trend towards increased TGF-β expression, indicating FITC-SPIF's potential in promoting macrophage polarization towards the M2 anti-inflammatory phenotype. This effect was consistent whether FITC-SPIF was used alone or released from the DDS, validating the efficacy of HAOX-CSOX hydrogels as carriers that preserve the bioactivity of FITC-SPIF (Fig. 5). High data variability underscores the necessity for a larger dataset. While *in vivo* studies have elucidated key functions of SPIF—such as immune modulation, embryo protection, and tissue repair—the precise molecular pathways remain unclear (Hayrabedyan et al., 2019; Ambrożkiewicz et al., 2022; Mueller et al., 2014). This knowledge gap complicates the accurate modelling of its therapeutic efficacy *in vitro*.

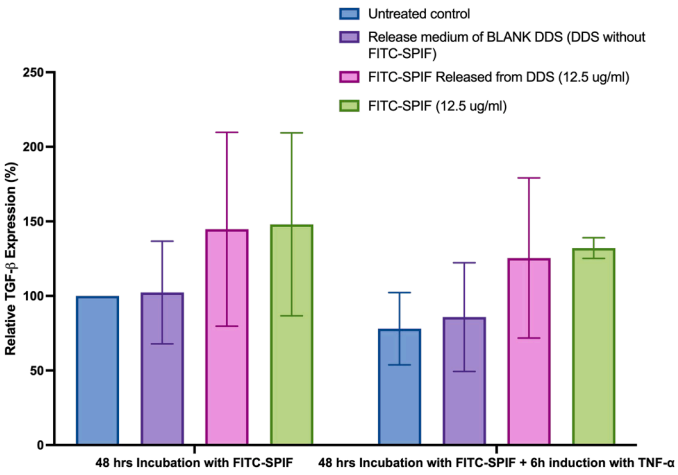

Fig. 5. TGF-β expression after treatment with SPIF.

Conclusion

This study investigates the versatility of an injectable hydrogel formulated from HAOX and CSOX as a DDS. The DDS consists of 2 % (w/v) HAOX and CSOX for the sustained release of 100 μg of FITC-SPIF. Key findings reveal a gelation time of 190 s, which is moderate for injectable systems, along with a low swelling profile of 18 %. The controlled release mechanism demonstrated an initial burst release reduction from 38 % at 0.5 % CSOX to 78 % at 1 % CSOX. This efffect contributed to extending of the release duration from 50 to 88 h with increased CSOX concentration. Also, this DDS operates within a clinically relevant dosing range by releasing FITC-SPIF at rates of 1–20 μg daily through anomalous transport mechanisms. This profile is expected to enhance control and consistency over treatment outcomes compared to traditional single-dosing regimens, potentially improving patient compliance and therapeutic efficacy.

Furthermore, electrostatic interactions between sulfate groups of CSOX and amine and guanidino residues of FITC-SPIF enhance drug entrapment by promoting binding without requiring organic solvents or chemical crosslinkers. The system can be administered through a 27 gauge needle, which is designed to minimize patient discomfort and reduce risks associated with device perforation compared to larger gauge needles. *In vitro* bioactivity tests confirm that the drug is compatible with the excipients used, validating its suitability for therapeutic potential. This validation, along with material selection and preparation methods, indicates an effective delivery system for FITC-SPIF. The collaborative effect among DDS components in sustaining FITC-SPIF release constitutes a transformative contribution in drug delivery technology so far unreported.

While the developed system shows promise, limitations include the absence of *in vivo* safety and efficacy assessments, which are crucial for its suitability clinical application. Currently, the research is in its early stages, focusing primarily on *in vitro* assessments to evaluate the feasibility and effectiveness of the DDS in controlled environments. It is recognized that results from *in vitro* studies may not directly translate to *in vivo* outcomes; however, based on previously established biocompatibility profiles, the degradation products from HAOX, CSOX, and PDHA are typically non-toxic and biocompatible, minimizing concerns about cytotoxicity. Comprehensive evaluations in preclinical models are necessary to confirm the therapeutic potential of this DDS for managing symptoms of chronic inflammatory diseases, such as MS. Future research may explore integrating this DDS into combination therapies with established MS medications to enhance treatment effectiveness and improve patient adherence. Overall, this hydrogel system presents a promising approach for enhancing SPIF delivery, with potential benefits in reducing dosing frequency and simplifying preparation methods.

CRediT authorship contribution statement

Tutut Habibah: Writing – review & editing, Writing – original draft, Visualization, Methodology, Investigation, Formal analysis, Conceptualization. **Andrea Exnerová:** Methodology, Investigation. **Kristina Nešporová:** Methodology, Conceptualization. **Una FitzGerald:** Funding acquisition, Conceptualization. **Abhay Pandit:** Writing – review & editing, Supervision. **Marek Ingr:** Supervision, Methodology. **Martin Pravda:** Writing – review & editing, Supervision, Methodology, Conceptualization. **Vladimír Velebný:** Funding acquisition.

Declaration of competing interest

The authors declare the following financial interests/personal relationships which may be considered as potential competing interests

Acknowledgments

This work was supported by the European Union's Horizon 2020 research and innovation programme under the Marie Skłodowska-Curie grant agreement no 813263. This publication has emanated from research supported partly by a grant from the Research Ireland and is co-funded under the European Regional Development Fund under grant number 13/RC/2073_P2.

Supplementary materials

Supplementary material associated with this article can be found, in the online version, at doi:10.1016/j.carpta.2025.100689.

Data availability

Data will be made available on request.

References

Agarwal, P., et al. (2021). Structural characterization and developability assessment of sustained release hydrogels for rapid implementation during preclinical studies. *European Journal of Pharmaceutical Sciences, 158*, 1–12. https://doi.org/10.1016/j.ejps.2020.105689

Alonso, J. M., Del Olmo, J. A., Gonzalez, R. P., & Saez-martinez, V. (2021). Injectable hydrogels: From laboratory to industrialization. *Polymers, 13*(4), 1–24. https://doi.org/10.3390/polym13040650

Ambrożkiewicz, K. A., Kozłowska, U., Haesler, V., Barnea, E. R., Mueller, M., & Kurpisz, M. (2022). Murine glial progenitor cells transplantation and synthetic PreImplantation Factor (sPIF) reduces inflammation and early motor impairment in ALS mice. *Scientific reports, 12*(1), 1–13. https://doi.org/10.1038/s41598-022-08064-9

Barnea, E. R., Kirk, D., Ramu, S., Rivnay, B., Roussev, R., & Paidas, M. J. (2012). PreImplantation factor (PIF) orchestrates systemic antiinflammatory response by immune cells: Effect on peripheral blood mononuclear cells. *American Journal of Obstetrics and Gynecology, 207*(4). https://doi.org/10.1016/j.ajog.2012.07.017. pp. 313.e1-313.e10.

Barone, D. A., Singer, B. A., Merkov, L., Rametta, M., & Suarez, G. (2016). Survey of US patients with multiple sclerosis: Comparison of the new electronic interferon beta-1b autoinjector (BETACONNECT™) with mechanical autoinjectors. *Neurology and Therapy, 5*(2), 155–167. https://doi.org/10.1007/s40120-016-0047-3

Bernhard, S., & Tibbitt, M. W. (2021). Supramolecular engineering of hydrogels for drug delivery. *Advanced Drug Delivery Reviews, 171*, 240–256. https://doi.org/10.1016/j.addr.2021.02.002

Berradi, A., Aziz, F., El Achaby, M., Ouazzani, N., & Mandi, L. (2023). A comprehensive review of polysaccharide-based hydrogels as promising biomaterials. *Polymers, 15*(13), 1–49. https://doi.org/10.3390/polym15132908

Bobula, T., et al. (2016). One-pot synthesis of α,β-unsaturated polyaldehyde of chondroitin sulfate. *Carbohydrate Polymers, 136*, 1002–1009. https://doi.org/10.1016/j.carbpol.2015.10.005

Bobula, T., Buffa, R., Hermannová, M., Vágnerová, H., Doleček ová, I., & Velebný, V. (2018). The synthesis of a new unsaturated derivative of chondroitin sulfate with increased antioxidant properties. *Carbohydrate Polymers, 190*, 175–183. https://doi.org/10.1016/j.carbpol.2018.02.080

Buenger, D., Topuz, F., & Groll, J. (2012). Hydrogels in sensing applications. *Progress in Polymer Science, 37*(12), 1678–1719. https://doi.org/10.1016/j.progpolymsci.2012.09.001

Buffa, R., et al. (2015). α,β-unsaturated aldehyde of hyaluronan - synthesis, analysis and applications. *Carbohydrate Polymers, 134*, 293–299. https://doi.org/10.1016/j.carbpol.2015.07.084

Cavaco, M., Valle, J., Flores, I., Andreu, D., & Castanho, M. A. R. B. (2021). Estimating peptide half-life in serum from tunable, sequence-related physicochemical properties. *Clinical and Translational Science, 14*(4), 1349–1358. https://doi.org/10.1111/cts.12985

Chen, Y. C., et al. (2016). Preimplantation factor prevents atherosclerosis via its immunomodulatory effects without affecting serum lipids. *Thrombosis and Haemostasis, 115*(5), 1010–1024. https://doi.org/10.1160/TH15-08-0640

Collins, J., Xiao, Z., Müllner, M., & Connal, L. A. (2016). The emergence of oxime click chemistry and its utility in polymer science. *Polymer Chemistry, 7*(23), 3812–3826. https://doi.org/10.1039/c6py00635c

Correale, J., Halfon, M. J., Jack, D., Rubstein, A., & Villa, A. (2021). Acting centrally or peripherally: A renewed interest in the central nervous system penetration of disease-modifying drugs in multiple sclerosis. *Multiple Sclerosis and Related Disorders, 56*, 1–10. https://doi.org/10.1016/j.msard.2021.103264

Di Simone, N., et al. (2017). Synthetic PreImplantation Factor (PIF) prevents fetal loss by modulating LPS induced inflammatory response. *PLoS One, 12*(7), 1–16. https://doi.org/10.1371/journal.pone.0180642

Dulong, V., Lack, S., Le Cerf, D., Picton, L., Vannier, J. P., & Muller, G. (2004). Hyaluronan-based hydrogels particles prepared by crosslinking with trisodium trimetaphosphate. Synthesis and characterization. *Carbohydrate Polymers, 57*(1), 1–6. https://doi.org/10.1016/j.carbpol.2003.12.006

Feng, W., & Wang, Z. (2023). Tailoring the swelling-shrinkable behavior of hydrogels for biomedical applications. *Advanced Science, 10*(28), 1–41. https://doi.org/10.1002/advs.202303326

Fitch, C. A., Platzer, G., Okon, M., Garcia-Moreno, B. E., & McIntosh, L. P. (2015). Arginine: Its pKa value revisited. *Protein Science, 24*(5), 752–761. https://doi.org/10.1002/pro.2647

Flory, P. J. (1953). *Principle of polymer chemistry, 1* pp. 432–584). USA: Cornell University Press.

Fu, Y., & Kao, W. J. (2010). Drug release kinetics and transport mechanisms of non-degradable and degradable polymeric delivery systems. *Expert Opinion on Drug Delivery, 7*(4), 429–444. https://doi.org/10.1517/17425241003602259

García-Couce, J., et al. (2021). Synthesis and evaluation of AlgNa-g-poly(QCL-co-HEMA) hydrogels as platform for chondrocyte proliferation and controlled release of betamethasone. *International Journal of Molecular Sciences, 22*(11), 1–17. https://doi.org/10.3390/ijms

Grover, G. N., Lam, J., Nguyen, T. H., Segura, T., & Maynard, H. D. (2012). Biocompatible hydrogels by oxime click chemistry. *Biomacromolecules, 13*(10), 3013–3017. https://doi.org/10.1021/bm301346e

Gummel, J., Cousin, F., & Boué, F. (2007). Counterions release from electrostatic complexes of polyelectrolytes and proteins of opposite charge: A direct measurement. *Journal of the American Chemical Society, 129*(18), 5806–5807. https://doi.org/10.1021/ja070414t

Habibah, T., et al. (2024). In situ formed aldehyde-modified hyaluronic acid hydrogel with polyelectrolyte complexes of aldehyde-modified chondroitin sulfate and gelatin: An approach for minocycline delivery. *Carbohydrate Polymers, 343*, 1–12. https://doi.org/10.1016/j.carbpol.2024.122455

Häusser-Kinzel, S., & Weber, M. S. (2019). The role of B cells and antibodies in multiple sclerosis, neuromyelitis optica, and related disorders. *Frontiers in Immunology, 10*(201), 1–6. https://doi.org/10.3389/fimmu.2019.00201

Hayrabedyan, S., et al. (2019). Synthetic PreImplantation Factor (sPIF) induces posttranslational protein modification and reverses paralysis in EAE mice. *Scientific Reports, 9*(1), 1–10. https://doi.org/10.1038/s41598-019-48473-x

Ho, T. C., et al. (2022). Hydrogels: Properties and applications in biomedicine. *MDPI, 27*(9), 1–29. https://doi.org/10.3390/molecules27092902

Hoti, G., et al. (2021). Effect of the cross-linking density on the swelling and rheological behavior of ester-bridged β-cyclodextrin nanosponges. *Materials, 14*(3), 1–20. https://doi.org/10.3390/ma14030478

Huang, X., & Brazel, C. S. (2001). On the importance and mechanisms of burst release in matrix-controlled drug delivery systems. *Journal of Controlled Release, 73*, 121–136. https://doi.org/10.1016/S0168-3659(01)00248-6

Ilgin, P., Ozay, H., & Ozay, O. (2019). A new dual stimuli responsive hydrogel: Modeling approaches for the prediction of drug loading and release profile. *European Polymer Journal, 113*, 244–253. https://doi.org/10.1016/j.eurpolymj.2019.02.003

Kesharwani, P., Bisht, A., Alexander, A., Dave, V., & Sharma, S. (2021). Biomedical applications of hydrogels in drug delivery system: An update. *Journal of Drug Delivery Science and Technology, 66*, 1–23. https://doi.org/10.1016/j.jddst.2021.102914

Knoerdel, A. R., Blocher McTigue, W. C., & Sing, C. E. (2021). Transfer matrix model of pH effects in polymeric complex coacervation. *Journal of Physical Chemistry B, 125*(31), 8965–8980. https://doi.org/10.1021/acs.jpcb.1c03065

Korsmeyer, R. W., Gurny, R., Doelker, E., Buri, P., & Peppas, N. A. (1983). Mechanisms of solute release from porous hydrophilic polymers. *International Journal of Pharmaceutics, 15*(1), 25–35. https://doi.org/10.1016/0378-5173(83)90064-9

Lavrentev, F. V., et al. (2023). Diffusion-limited processes in hydrogels with chosen applications from drug delivery to electronic components. *Molecules (Basel, Switzerland), 28*(15), 1–32. https://doi.org/10.3390/molecules28155931

Lei, L., Bai, Y., Qin, X., Liu, J., Huang, W., & Lv, Q. (2022). Current understanding of hydrogel for drug release and tissue engineering. *Gels, 8*(5), 1–31. https://doi.org/10.3390/gels8050301

Li, J., & Mooney, D. J. (2016). Designing hydrogels for controlled drug delivery. *Nature Publishing Group, 1*(12), 1–17. https://doi.org/10.1038/natrevmats.2016.71

Lin, G., Chang, S., Kuo, C. H., Magda, J., & Solzbacher, F. (2009). Free swelling and confined smart hydrogels for applications in chemomechanical sensors for physiological monitoring. *Sensors and Actuators. B, Chemical, 136*(1), 186–195. https://doi.org/10.1016/j.snb.2008.11.001

Lin, X., Zhao, X., Xu, C., Wang, L., & Xia, Y. (2022). Progress in the mechanical enhancement of hydrogels: Fabrication strategies and underlying mechanisms. *Journal of Polymer Science, 60*(17), 2525–2542. https://doi.org/10.1002/pol.20220154

Lin, Y. T., Will, T., Wickham, C., Boeree, P., Jack, D., & Keiser, M. (2023). Evolution of the RebiSmart® electromechanical autoinjector to improve usability in support of adherence to subcutaneous interferon beta-1a therapy for people living with Multiple sclerosis. *Patient Preference and Adherence, 17*, 1923–1933. https://doi.org/10.2147/PPA.S414151

Ma, X., Ma, R., Zhang, M., Qian, B., Wang, B., & Yang, W. (2023). Recent progress in multiple sclerosis treatment using immune cells as targets. *Pharmaceutics, 15*(728), 1–20. https://doi.org/10.3390/pharmaceutics15030728

Marciel, A. B., Chung, E. J., Brettmann, B. K., & Leon, L. (2017). Bulk and nanoscale polypeptide based polyelectrolyte complexes. *Advances in Colloid and Interface Science, 239*, 187–198. https://doi.org/10.1016/j.cis.2016.06.012

Martini, M., et al. (2016). Charged triazole cross-linkers for hyaluronan-based hybrid hydrogels. *Materials, 9*(10), 1–11. https://doi.org/10.3390/ma9100810

Meyer-Arndt, L., et al. (2023). Inflammatory cytokines associated with multiple sclerosis directly induce alterations of neuronal cytoarchitecture in Human neurons. *Journal of Neuroimmune Pharmacology, 18*(1–2), 145–159. https://doi.org/10.1007/s11481-023-10059-w

Mihajlovic, M., et al. (2022). Viscoelastic chondroitin sulfate and hyaluronic acid double-network hydrogels with reversible cross-links. *Biomacromolecules, 23*(3), 1350–1365. https://doi.org/10.1021/acs.biomac.1c01583

Mikulík, J., Vinklárek, Z., & Vondruška, M. (1993). Formation of polyelectrolyte complexes. *Collection of Czechoslovak Chemical Communications, 58*(4), 713–747. https://doi.org/10.1135/cccc19930713

Modrzejewska, Z., Nawrotek, K., & Zarzycki, R. (2010). Drug release from hydrogel matrices. *Ecological Chemistry and Engineering S, 17*(2), 117–136.

Mueller, M., et al. (2014). Prelmplantation factor promotes neuroprotection by targeting microRNA let-7. *Proceedings of the National Academy of Sciences of the United States of America, 111*(38), 13882–13887. https://doi.org/10.1073/pnas.1411674111

Niemczyk, B., Sajkiewicz, P., & Kolbuk, D. (2018). Injectable hydrogels as novel materials for central nervous system regeneration. *Journal of Neural Engineering, 15*(5), 1–15. https://doi.org/10.1088/1741-2552/aacbab

Novoskol'tseva, O. A., Rogacheva, V. B., Zezin, A. B., Joosten, J., & Brackman, J. (2009). Formation and transformations of polyelectrolyte gel-ampholyte dendrimer-surfactant ternary complexes. *Polymer Science - Series A, 51*(6), 598–605. https://doi.org/10.1134/S0965545×09060030

O'Brien, C. B., et al. (2018). Randomized, double-blind, placebo-controlled, single ascending dose trial of synthetic preimplantation factor in autoimmune Hepatitis. *Hepatology Communications, 2*(10), 1235–1246. https://doi.org/10.1002/hep4.1239

Peppas, N. A., Bures, P., Leobandung, W., & Ichikawa, H. (2000). Hydrogels in pharmaceutical formulations. *European Journal of Pharmaceutics and Biopharmaceutics, 50*(1), 27–46. https://doi.org/10.1016/S0939-6411(00)00090-4

Qu, K., et al. (2022). Structures, properties, and applications of zwitterionic polymers. *ChemPhysMater, 1*(4), 294–309. https://doi.org/10.1016/j.chphma.2022.04.003

Rungrod, A., Kapanya, A., Punyodom, W., Molloy, R., Mahomed, A., & Somsunan, R. (2022). Synthesis and characterization of semi-IPN hydrogels composed of sodium 2-acrylamido-2-methylpropanesulfonate and poly(ε-caprolactone) diol for controlled

drug delivery. *European Polymer Journal, 164*, 1–18. https://doi.org/10.1016/j.eurpolymj.2021.110978

Salehi, S., Naghib, S. M., Garshasbi, H. R., Ghorbanzadeh, S., & Zhang, W. (2023). Smart stimuli-responsive injectable gels and hydrogels for drug delivery and tissue engineering applications: A review. *Frontiers in Bioengineering and Biotechnology, 11*, 1–20. https://doi.org/10.3389/fbioe.2023.1104126

Samantray, S., Olubiyi, O. O., & Strodel, B. (2021). The influences of sulphation, salt type, and salt concentration on the structural heterogeneity of glycosaminoglycans. *International Journal of Molecular Sciences, 22*(21), 1–20. https://doi.org/10.3390/ijms222111529

Schatz, C., Domard, A., Viton, C., Pichot, C., & Delair, T. (2004). Versatile and efficient formation of colloids of biopolymer-based polyelectrolyte complexes. *Biomacromolecules, 5*, 1882–1892. https://doi.org/10.1021/bm049786

Šedová, P., et al. (2022). The effect of aminooxy-linkers' structure on the mechanical properties of hyaluronan-oxime hydrogels. *EXPRESS Polymer Letters, 16*(3), 265–278. https://doi.org/10.3144/EXPRESSPOLYMLETT.2022.21

Shah, S., & Leon, L. (2021). Structural dynamics, phase behavior, and applications of polyelectrolyte complex micelles. *Current Opinion in Colloid & Interface Science, 53*, 1–12. https://doi.org/10.1016/j.cocis.2021.101424

Shimojo, A. A. M., Pires, A. M. B., Lichy, R., Rodrigues, A. A., & Santana, M. H. A. (2015). The crosslinking degree controls the mechanical, rheological, and swelling properties of hyaluronic acid microparticles. *Journal of Biomedical Materials Research. Part A, 103*(2), 730–737. https://doi.org/10.1002/jbm.a.35225

Spinelli, M., et al. (2020). Synthetic PreImplantation Factor (sPIF) reduces inflammation and prevents preterm birth. *PLoS One, 15*(6), 1–14. https://doi.org/10.1371/journal.pone.0232493

Stojkov, G., Niyazov, Z., Picchioni, F., & Bose, R. K. (2021). Relationship between structure and rheology of hydrogels for various applications. *Gels, 7*(4), 1–20. https://doi.org/10.3390/gels7040255

Takeno, H., & Sato, C. (2016). Effects of molecular mass of polymer and composition on the compressive properties of hydrogels composed of laponite and sodium polyacrylate. *Applied Clay Science, 123*, 141–147. https://doi.org/10.1016/j.clay.2016.01.030

Takeshita, Y., & Ransohoff, R. M. (2012). Inflammatory cell trafficking across the blood-brain barrier: Chemokine regulation and in vitro models. *Immunological Reviews, 248*(1), 228–239. https://doi.org/10.1111/j.1600-065X.2012.01127.x

Tanaka, K. (1978). Physicochemical properties of chondroitin sulfate. *The Journal of Biochemistry, 83*(3), 647–653. https://doi.org/10.1093/oxfordjournals.jbchem.a131955

Tao, Y., Ai, L., Bai, H., & Liu, X. (2012). Synthesis of pH-responsive photocrosslinked hyaluronic acid-based hydrogels for drug delivery. *Journal of Polymer Science. Part A, Polymer Chemistry, 50*(17), 3507–3516. https://doi.org/10.1002/pola.26159

Toropitsyn, E., Ščigalková, I., Pravda, M., & Velebný, V. (2023). Injectable hyaluronic acid hydrogel containing platelet derivatives for synovial fluid viscosupplementation and growth factors delivery. *Macromolecular Bioscience, 23*(4), 1–14. https://doi.org/10.1002/mabi.202200516

Touil, H., et al. (2023). Cross-talk between B cells, microglia and macrophages, and implications to central nervous system compartmentalized inflammation and progressive multiple sclerosis. *EBioMedicine, 96*(104789), 1–15. https://doi.org/10.1016/j.ebiom.2023.104789

Tseng, T. C., Tao, L., Hsieh, F. Y., Wei, Y., Chiu, I. M., & Hsu, S. H. (2015). An injectable, self-healing hydrogel to repair the central nervous system. *Advanced Materials, 27*(23), 3518–3524. https://doi.org/10.1002/adma.201500762

Visser, L. A., Huls, S. P. I., Uyl-de Groot, C. A., de Bekker-Grob, E. W., & Redekop, W. K. (2021). An implantable device to treat multiple sclerosis: A discrete choice experiment on patient preferences in three European countries. *Journal of the Neurological Sciences, 428*, 1–11. https://doi.org/10.1016/j.jns.2021.117587

Wang, L., et al. (2022). Therapeutic peptides: Current applications and future directions. *Signal Transduction and Targeted Therapy, 7*(1), 1–18. https://doi.org/10.1038/s41392-022-00904-4

Weiss, L., et al. (2012). Preimplantation Factor (PIF*) reverses neuroinflammation while promoting neural repair in EAE model. *Journal of the Neurological Sciences, 312*(1–2), 146–157. https://doi.org/10.1016/j.jns.2011.07.050

Wu, D., Chen, Q., Chen, X., Han, F., Chen, Z., & Wang, Y. (2023). The blood–brain barrier: Structure, regulation, and drug delivery. *Signal Transduction and Targeted Therapy, 8*(217), 1–20. https://doi.org/10.1038/s41392-023-01481-w

Xue, Y., Chen, H., Xu, C., Yu, D., Xu, H., & Hu, Y. (2020). Synthesis of hyaluronic acid hydrogels by crosslinking the mixture of high-molecular-weight hyaluronic acid and low-molecular-weight hyaluronic acid with 1,4-butanediol diglycidyl ether. *RSC Advances, 10*(12), 7206–7213. https://doi.org/10.1039/c9ra09271d

Yang, C., Hawkins, K. E., Doré, S., & Candelario-Jalil, X. E. (2019). Neuroinflammatory mechanisms of blood-brain barrier damage in ischemic stroke. *American Journal of Physiology, 316*, 135–153. https://doi.org/10.1152/ajp

Zhang, Z., He, C., & Chen, X. (2018). Hydrogels based on pH-responsive reversible carbon-nitrogen double-bond linkages for biomedical applications. *Materials Chemistry Frontiers, 2*(10), 1765–1778. https://doi.org/10.1039/c8qm00317c

Zhuo, F., Liu, X., Gao, Q., Wang, Y., Hu, K., & Cai, Q. (2017). Injectable hyaluronan-methylcellulose composite hydrogel crosslinked by polyethylene glycol for central nervous system tissue engineering. *Materials Science and Engineering C, 81*, 1–7. https://doi.org/10.1016/j.msec.2017.07.029